Interleukin 18 function in atherosclerosis is mediated by the interleukin 18 receptor and the Na-Cl co-transporter

Interleukin 18 function requires both interleukin 18 receptor and Na-Cl co-transporter

Jing Wang,[1,2*] Chongxiu Sun,[1*] Norbert Gerdes,[1,3] Conglin Liu,[1,4] Mengyang Liao,[1,5] Jian Liu,[1] Michael A. Shi,[1] Aina He,[1] Yi Zhou,[1] Galina K. Sukhova,[1] Huimei Chen,[1] Xianwu Cheng,[6] Masafumi Kuzuya,[6] Toyoaki Murohara,[6] Jie Zhang,[1] Xiang Cheng,[1,5] Mengmeng Jiang,[7] Gary E. Shull,[7] Shaunessy Rogers,[8] Chao-Ling Yang,[8] Qiang Ke,[1] Sabina Jelen,[9] René Bindels,[9] David H. Ellison,[8] Petr Jarolim,[10] Peter Libby,[1] and Guo-Ping Shi[1]

1. Department of Medicine, Brigham and Women's Hospital and Harvard Medical School, Boston, MA, USA
2. State Key Laboratory of Medical Molecular Biology, Institute of Basic Medical Sciences, Chinese Academy of Medical Sciences, Department of Pathophysiology, Peking Union Medical College, Tsinghua University, Beijing 100005, China
3. Institute for Cardiovascular Prevention (IPEK), Ludwig-Maximilians University Munich, Pettenkoferstrasse 9, 80336 Munich, Germany
4. Institute of Clinical Medicine, the First Affiliated Hospital of Zhengzhou University, Zhengzhou, China
5. Institute of Cardiology, Union Hospital, Tongji Medical College of Huazhong University of Science and Technology, Wuhan, China
6. Departments of Cardiology and Geriatrics, Graduate School of Medicine, Nagoya University, Japan
7. Department of Molecular Genetics, Biochemistry, and Microbiology, University of Cincinnati College of Medicine, Cincinnati, OH, USA
8. Division of Nephrology and Hypertension, Oregon Health and Science University, and VA Medical Center, Portland, OR, USA
9. Department of Physiology, Radboud University Nijmegen Medical Centre, 6500 HB Nijmegen, The Netherlands
10. Department of Pathology, Brigham and Women's Hospital and Harvard Medical School, Boston, MA, USA

* These authors contributed equally to this study.

Running title: Na-Cl co-transporter and IL18 function

Corresponding Author:

Guo-Ping Shi, D.Sc.
Cardiovascular Medicine
77 Avenue Louis Pasteur, NRB-7
Boston, MA 02115
Email: gshi@rics.bwh.harvard.edu

Interleukin-18 (IL18) participates in atherogenesis through several putative mechanisms[1,2]. Interruption of IL18 action reduces atherosclerosis in mice[3,4]. This study shows that the absence of IL18 receptor (IL18r) does not affect atherosclerosis in apolipoprotein E-deficient (*Apoe*$^{-/-}$) mice, nor does it affect IL18 cell surface binding or signaling. IL18 antibody-mediated immunoprecipitation identified an interaction between IL18 and Na-Cl co-transporter (NCC), a 12-transmembrane-domain ion transporter protein preferentially expressed in the kidney[5]. Yet, we find NCC expression and colocalization with IL18r in atherosclerotic lesions and both molecules form a complex. IL18 also binds to the cell surface and induces cell signaling and down-stream cytokine expression in NCC-transfected COS-7 cells that do not express IL18r. In *Apoe*$^{-/-}$ mice, combined deficiency of IL18r and NCC, but not single deficiency, protects mice from atherosclerosis. Peritoneal macrophages from *Apoe*$^{-/-}$ mice or those lacking IL18r or NCC respond to IL18 binding or IL18 induction of cell signaling and cytokine and chemokine production, but those with combined deficiency of IL18r and NCC do not. This study identifies NCC as an IL18-binding protein that coordinates with IL18r in cell signaling, inflammatory molecule expression, and experimental atherogenesis.

IL18 polarizes Th1 cells[1,2] and induces production of inflammatory cytokines, chemokines, and vascular adhesion molecules[2,6-8]. Prior studies with mice deficient in IL18 (*Il18*$^{-/-}$), its receptor IL18r (*Il18r*$^{-/-}$), or soluble receptors demonstrate the contribution of IL18 to several inflammatory diseases[9-11]. Atherosclerotic lesions but not normal human aortas express high levels of IL18 and IL18r in macrophages, T cells,

endothelial cells (ECs), and smooth-muscle cells (SMCs)[12,13]. In atherosclerosis-prone apolipoprotein E–deficient (*Apoe*$^{-/-}$) mice, the absence of IL18 or blockade of IL18 signaling reduces atherosclerosis and lesion inflammation[3,4]. Intraperitoneal administration of IL18 in *Apoe*$^{-/-}$ mice enhances lesion burden and inflammation[14,15]. IL18r is a heterodimer with a low IL18-binding affinity[16]. Absence of IL18r leads to reduced NK cell IFN-γ production and impaired Th1 cell signaling and differentiation[17]. Yet, *Apoe*$^{-/-}$ and *Apoe*$^{-/-}$*Il18r*$^{-/-}$ littermates showed no differences in atherogenesis. In *Apoe*$^{-/-}$ mice, the presence or absence of IL18r did not affect aortic root intimal area, or lesion macrophage, CD4^{+} T-cell, or SMC contents (**Fig. 1a**) — suggesting IL18 action on target cells that is independent of, or in addition to, the known IL18r. Mouse ECs from *Apoe*$^{-/-}$ and *Apoe*$^{-/-}$*Il18r*$^{-/-}$ mice incubated with biotinylated IL18, showed no differences in cell surface IL18 binding, competable by a 5~10-fold excess of unlabeled IL18 (**Fig. 1b**). ECs from *Apoe*$^{-/-}$ and *Apoe*$^{-/-}$*Il18r*$^{-/-}$ mice showed a similar pattern of protein tyrosine phosphorylation after 30 minutes of incubation with IL18, as detected by immunoblot with anti-phospho (p)-tyrosine antibody. Heat-inactivated IL18 did not elicit these activities (**Fig. 1c**). These data pointed to the presence of alternative molecules that mediate cell-surface IL18 binding and downstream signaling. Incubation of ECs from *Apoe*$^{-/-}$*Il18r*$^{-/-}$ mice with IL18 for 15 minutes followed by immunoprecipitation with an anti-mouse IL18 polyclonal antibody identified possible cell-surface IL18-binding molecules. Silver-stained SDS-PAGE showed two major bands between 85 to 150 kDa in series eluates from IL18-treated ECs (**Fig. 1d**). Mass spectrometry identified a 125-kDa Na-Cl co-transporter (NCC) in addition to multiple matrix protein fragments (data not shown).

NCC is a plasma membrane ion co-transporter expressed as a homodimer in kidney distal convoluted tubules, where it participates in electrolyte homeostasis[18], although other tissues express low levels of NCC[5,19]. We detected abundant NCC mRNA in mouse kidney, but also low levels in the heart, lung, and liver by RT-PCR (**Supplementary Fig. 1**). Immunostaining using an anti-human/mouse NCC polyclonal antibody revealed no NCC expression in normal human or mouse aortas (**Fig. 2a**), but abundant NCC expression in human fatty streaks (**Supplementary Fig. 2**) and advanced atherosclerotic lesions (**Fig. 2b**), localized to areas positive for IL18r and $CD68^+$ macrophages. Tests of antibody specificity confirmed NCC expression in kidney distal tubules from *Apoe*$^{-/-}$ mice, but not in those from *Apoe*$^{-/-}$*Ncc*$^{-/-}$ mice (**Supplementary Fig. 3**). Macrophages, SMCs, and ECs in atherosclerotic lesions from *Apoe*$^{-/-}$ mice expressed NCC (**Fig. 2c**). Immunofluorescent staining confirmed colocalization of NCC and IL18r in macrophages, SMCs, and ECs in lesions from *Apoe*$^{-/-}$ mice (**Fig. 2d**). RT-PCR demonstrated that IL18 induced NCC expression in mouse peritoneal macrophages by 65-fold, but had negligible effect on T cells. Immunostaining revealed induction of NCC by IL18 in macrophages and T cells from *Apoe*$^{-/-}$ mice (**Fig. 2e**). Immunoblot showed that IL18, IL1β, or TNF-α increased NCC expression in mouse ECs and SMCs, with the same molecular weight as those expressed in NCC/pcDNA3.1-transfected COS-7 cells (**Fig. 2f**). Immunoprecipitation with mouse anti-mouse IL18r antibody followed by immunoblot with the rabbit anti-mouse NCC antibody in macrophage lysates demonstrated an enhanced complex formation between IL18r and NCC in IL18-treated macrophages from *Apoe*$^{-/-}$ mice but not those from *Apoe*$^{-/-}$*Ncc*$^{-/-}$ mice (**Fig. 2g**). To study NCC and its interaction with IL18, we subcloned NCC full-length cDNA into a

pcDNA3.1 vector. Immunoblot revealed mouse NCC in NCC-transfected COS-7 cells as a doublet band around 125-kDa, due to differential protein glycosylations (**Supplementary Fig. 4**)[18]. FACS analysis demonstrated surface binding of biotin-conjugated IL18, but not heat-inactivated biotin-IL18 on NCC-transfected COS-7 cells 30 minutes after induction (**Fig. 2h**). FITC-conjugated IL18 binding to NCC-transfected COS-7 cells, which do not express IL18r in the presence or absence of IL18 (data not shown), showed a higher binding affinity (dissociation constant K_d = 17.3 nM) than previously reported IL18 binding on IL18r-transfected COS-1 cells (K_d = 46 nM)[16] (**Fig. 2h**). Treatment with IL18, but not heat-inactivated IL18 for 30 minutes also increased protein tyrosine phosphorylation in NCC-transfected COS-7 cells, compared with those transfected with empty vector (**Fig. 2h**), indicating that IL18 interacts with NCC and yields biological consequences.

Insignificant differences in atherogenesis between *Apoe*$^{-/-}$ and *Apoe*$^{-/-}$*Il18r*$^{-/-}$ mice (**Fig. 1a**) and binding of IL18 on NCC-transfected COS-7 cells and consequent cell signaling (**Fig. 2h**) suggest that NCC mediates IL18 functions in atherogenesis in the presence and absence of IL18r. To test this hypothesis, we crossbred NCC-deficient mice (*Ncc*$^{-/-}$, on a C57BL/6/129S background)[20] with *Apoe*$^{-/-}$ and *Il18r*$^{-/-}$ mice and generated *Apoe*$^{-/-}$*Ncc*$^{-/-}$, *Apoe*$^{-/-}$*Il18r*$^{-/-}$, and *Apoe*$^{-/-}$*Ncc*$^{-/-}$*Il18r*$^{-/-}$ littermate mice with their background identity confirmed with a genome scanning analysis (data not shown). Compared with *Apoe*$^{-/-}$ and *Apoe*$^{-/-}$*Il18r*$^{-/-}$ mice (**Fig. 1a**), *Apoe*$^{-/-}$*Ncc*$^{-/-}$ mice showed no significant differences in aortic root atherosclerotic lesion intima area and thoracic-abdominal aorta lipid deposition, although this study did not characterize lesions from the aortic arches. In contrast, aortic root intimal size ($P < 0.001$) and thoracic-abdominal

aorta lipid deposition ($P < 0.002$) decreased significantly in *Apoe*$^{-/-}$*Ncc*$^{-/-}$*Il18r*$^{-/-}$ mice (**Fig. 3a/3b**), suggesting that IL18r and NCC coordinately mediate IL18 function. IL18r may compensate the NCC loss of function, and *vice versa*. Lesion Mac-3^{+} macrophage content ($P < 0.001$), major histocompatibility class-II (MHC-II)–positive areas ($P < 0.002$), and α-actin–positive SMC areas ($P < 0.01$) also decreased significantly in *Apoe*$^{-/-}$*Ncc*$^{-/-}$*Il18r*$^{-/-}$ mice but not in *Apoe*$^{-/-}$*Il18r*$^{-/-}$ or *Apoe*$^{-/-}$*Ncc*$^{-/-}$ mice, compared with *Apoe*$^{-/-}$ mice (**Fig. 3c/3d**). Lesion CD4^{+} T cell numbers did not differ between the groups (**Fig. 3c**). Aortic root lesion lipid deposition (**Fig. 3e**) decreased in *Apoe*$^{-/-}$*Il18r*$^{-/-}$ mice ($P = 0.079$), and significantly decreased in *Apoe*$^{-/-}$*Ncc*$^{-/-}$ mice ($P < 0.02$), but *Apoe*$^{-/-}$*Ncc*$^{-/-}$*Il18r*$^{-/-}$ mice showed a greater decrease ($P < 0.003$). NCC inactivation with a thiazide diuretic (hydrochlorothiazide) in *Apoe*$^{-/-}$ and *Apoe*$^{-/-}$*Il18r*$^{-/-}$ mice affirmed a modulatory role for IL18 in atherosclerosis mediated by IL18r and NCC. Thiazide reduced aortic root lesion intima area, lesion macrophage and MHC-II contents in *Apoe*$^{-/-}$*Il18r*$^{-/-}$mice but not in *Apoe*$^{-/-}$ mice. Thiazide showed no effect on lesion CD4^{+} T cell content (**Supplementary Fig. 5a**). Consistent with prior observations[14,15], IL18 administration to *Apoe*$^{-/-}$ mice accentuated atherogenesis with increased intima size and lesion macrophage and MHC-II content, although IL18 did not affect lesion T cell number. In contrast, IL18 lacked these effects in *Apoe*$^{-/-}$*Ncc*$^{-/-}$*Il18r*$^{-/-}$ mice (**Supplementary Fig. 5b**). Prior studies[3] and our unpublished observation (data not shown) demonstrated significantly increased plasma cholesterol ($P < 0.001$) and triglyceride ($P < 0.01$) in IL18-deficeint *Apoe*$^{-/-}$ mice. *Apoe*$^{-/-}$*Il18r*$^{-/-}$ mice also had increased plasma cholesterol and triglyceride compared with *Apoe*$^{-/-}$ mice. *Apoe*$^{-/-}$*Ncc*$^{-/-}$*Il18r*$^{-/-}$ mice, however, had significantly increased plasma HDL ($P < 0.003$) and decreased LDL ($P = 0.025$) (**Supplementary Fig. 6**).

In humans and mice, defective NCC leads to hypomagnesemia, hypokalemia, or metabolic alkalosis[21,22], kidney tubular disorders that can influence atherosclerosis indirectly[23]. IL18 actions on the plaque itself may not solely determine reduced atherosclerosis in *Apoe*$^{-/-}$*Ncc*$^{-/-}$*Il18r*$^{-/-}$ mice. *Apoe*$^{-/-}$*Ncc*$^{-/-}$ ($P < 0.001$) and *Apoe*$^{-/-}$*Ncc*$^{-/-}$ *Il18r*$^{-/-}$ ($P < 0.001$) mice both had significantly reduced plasma Mg^{2+}, whereas only *Apoe*$^{-/-}$*Ncc*$^{-/-}$*Il18r*$^{-/-}$ mice ($P = 0.005$) had reduced plasma K^+. Plasma pH did not differ among the four groups of mice (**Supplementary Fig. 7**). *Apoe*$^{-/-}$ and *Apoe*$^{-/-}$*Ncc*$^{-/-}$ mice had similar atherosclerotic lesions sizes (**Fig. 3a/3b**), minimizing the confounding effects of hypomagnesemia or metabolic alkalosis on atherosclerosis in *Apoe*$^{-/-}$*Ncc*$^{-/-}$*Il18r*$^{-/-}$ mice, although the role of hypokalemia in atherosclerosis remains unknown. Bone marrow transplantation (BMT) from *Apoe*$^{-/-}$*Ncc*$^{-/-}$*Il18r*$^{-/-}$ mice demonstrated significantly smaller aortic root intima areas ($P = 0.002$), thoracic-abdominal aorta lipid deposition ($P = 0.024$), aortic root lesion content of macrophages ($P = 0.009$) and lipids ($P = 0.02$), and plasma total cholesterol ($P = 0.046$) and LDL ($P = 0.04$) in *Apoe*$^{-/-}$*Ncc*$^{-/-}$*Il18r*$^{-/-}$ recipient mice than those receiving BMT from *Apoe*$^{-/-}$ or *Apoe*$^{-/-}$*Il18r*$^{-/-}$ mice. Yet, *Apoe*$^{-/-}$*Ncc*$^{-/-}$ *Il18r*$^{-/-}$ recipient mice that received bone marrow from the various mutant mice showed no significant differences in aortic root lesion T-cell number, MHC class-II-positive area, SMC content, or plasma K^+, Mg^{2+}, or pH (**Fig. 3a-3e** and **Supplementary Fig. 6/7**). These observations suggest that IL18r- and NCC-mediated IL18 activation of bone marrow-derived leukocytes and possibly vascular cells, rather than kidney tubular disorders or electrolyte disturbances, engendered reduced atherosclerosis in *Apoe*$^{-/-}$*Ncc*$^{-/-}$ *Il18r*$^{-/-}$ mice.

IL18 induces cytokine expression in inflammatory diseases[2,3,6,15]. Serum IL18 levels in human subjects with atherosclerosis correlate with carotid intima thickness and other biomarkers of inflammation[24,25]. *Apoe*$^{-/-}$*Ncc*$^{-/-}$*Il18r*$^{-/-}$ mice showed the greatest reductions of plasma IFN-γ, IL6, and IL18, compared with the other three groups of mice, although *Apoe*$^{-/-}$*Il18r*$^{-/-}$ or *Apoe*$^{-/-}$*Ncc*$^{-/-}$ mice also had lower plasma IL6 and/or IL18 (**Fig. 3f**). These findings suggest that both IL18r and NCC contribute to IL18-induced cytokine production. BMT of *Apoe*$^{-/-}$*Ncc*$^{-/-}$*Il18r*$^{-/-}$ recipient mice supported this hypothesis. *Apoe*$^{-/-}$*Ncc*$^{-/-}$*Il18r*$^{-/-}$ recipient mice receiving BMT from *Apoe*$^{-/-}$*Ncc*$^{-/-}$*Il18r*$^{-/-}$ mice showed significantly lower plasma IFN-γ ($P = 0.026$), IL6 ($P = 0.012$), and IL18 ($P = 0.004$) than mice receiving BMT from *Apoe*$^{-/-}$ and *Apoe*$^{-/-}$*Il18r*$^{-/-}$ mice (**Fig. 3f**). Although the T cell content of lesions from mice of the different genotypes or from *Apoe*$^{-/-}$*Ncc*$^{-/-}$*Il18r*$^{-/-}$ mice receiving BMT from different donors did not differ (**Fig. 3c**), IL18r and NCC expression determined IL18-induced IFN-γ and IL6 production from T cells. IL18 with or without IL12, which augments IL18 actions by inducing targeting cell IL18r expression and Th1 cell differentiation[6,26], induced IFN-γ and IL6 expression in T cells from *Apoe*$^{-/-}$ mice. In contrast, production of both cytokines declined in T cells from *Apoe*$^{-/-}$*Ncc*$^{-/-}$ and *Apoe*$^{-/-}$*Il18r*$^{-/-}$, and declined further in *Apoe*$^{-/-}$*Ncc*$^{-/-}$*Il18r*$^{-/-}$ mice (**Fig. 3g**).

Macrophages also elaborate circulating cytokines. Recombinant IL18 promotes atherogenesis and enhances circulating cytokine levels in the absence of T cells[14,15]. Macrophages express IL18r and NCC in atherosclerotic lesions or after stimulation with inflammatory mediators (**Fig. 2b-2e**)[12,13]. NCC may mediate IL18 actions on macrophages in the absence of IL18r, and *vice versa*. FITC-conjugated IL18 binding to

NCC on macrophages (from *Apoe*$^{-/-}$*Il18r*$^{-/-}$ mice) showed a similar binding affinity (K_d = 21.39 nM) (**Fig. 4a**) to that of IL18 to IL18r on cells of human lymphoma line L428 (K_d = 18.5 nM)[4]. When treated with IL18, macrophages from *Apoe*$^{-/-}$, *Apoe*$^{-/-}$*Ncc*$^{-/-}$, or *Apoe*$^{-/-}$*Il18r*$^{-/-}$ mice showed phosphorylation of extracellular-signal–regulated kinases (ERK1/2) and p38 mitogen-activated protein kinase (MAPK) — regulators of cell growth, proliferation, differentiation, and inflammatory responses[27,28]. Yet, macrophages from *Apoe*$^{-/-}$*Ncc*$^{-/-}$*Il18r*$^{-/-}$ mice exposed to IL18 showed neither ERK1/2 nor p38 phosphorylation (**Fig. 4b**), suggesting that IL18r and NCC cooperatively mediate IL18 binding and cell signaling. Consistently, IL18 augmented IL6, IFN-γ, and monocyte chemotactic protein-1 (MCP-1) mRNA (**Supplementary Fig. 8**) and culture media protein levels (**Fig. 4c/d**) in macrophages from *Apoe*$^{-/-}$, *Apoe*$^{-/-}$*Ncc*$^{-/-}$, or *Apoe*$^{-/-}$*Il18r*$^{-/-}$ mice, but macrophages from *Apoe*$^{-/-}$*Ncc*$^{-/-}$*Il18r*$^{-/-}$ mice showed a mild or negligible response to IL18. NCC blockade with a thiazide diuretic affirmed a coordinate role of NCC and IL18r in response to IL18 in macrophages. Hydrochlorothiazide treatment of macrophages from *Apoe*$^{-/-}$*Il18r*$^{-/-}$ mice lowered the culture medium IL6 to the same level as in cells from *Apoe*$^{-/-}$*Ncc*$^{-/-}$*Il18r*$^{-/-}$ mice, but did not yield further reduction in cells from *Apoe*$^{-/-}$*Ncc*$^{-/-}$*Il18r*$^{-/-}$ mice (**Fig. 4d**). In macrophages from *Apoe*$^{-/-}$*Il18r*$^{-/-}$ mice, hydrochlorothiazide reduced ERK1/2 phosphorylation, but had negligible effect in cells from *Apoe*$^{-/-}$ mice (**Fig. 4d**). STE20/SPS-1-related proline-alanine-rich protein kinase (SPAK) can activate NCC[29]. IL18 induced SPAK phosphorylation in macrophages from *Apoe*$^{-/-}$, *Apoe*$^{-/-}$*Ncc*$^{-/-}$, and *Apoe*$^{-/-}$*Il18r*$^{-/-}$ mice, but not in cells from *Apoe*$^{-/-}$*Ncc*$^{-/-}$*Il18r*$^{-/-}$ mice (**Fig. 4e**). Therefore, IL18-induced SPAK phosphorylation also required both NCC and IL18r. IL18-induced cytokine expression difference among IL1β and TNF-α-pre-

treated macrophages from all four groups of mice (**Fig. 4c/4d**) was specific to IL18. TGF-β1 induced macrophage IL6 production independent of IL18r and NCC genotypes (data not shown).

The treatment of NCC-transfected COS-7 cells with IL18, with or without IL12, provided further evidence that NCC contributes to IL18 signaling and inflammatory cytokine production. NCC over-expression may affect cell volume[30] and intracellular Cl^- levels[31], and thereby affect cell signaling independent of IL18 binding[31,32]. NCC over-expression yielded significantly enlarged COS-7 cell volume ($P = 0.003$), but did not change intracellular Cl^- concentrations before or after NaCl addition, suggesting the integrity of NCC-expressing COS-7 cells (**Supplementary Fig. 9**)[33]. Increased cell volume may have caused higher baseline phosphorylation of the transcription factor STAT-3[34] and p38 MAPK in NCC-transfected COS-7 cells than in vector-transfected COS-7 cells (**Fig. 4f**). IL18 alone or in combination with IL12, however, induced phosphorylation of STAT-3 and p38 in NCC-transfected cells in 15~30 minutes, but not in vector-transfected cells (**Fig. 4f**). When three NCC point mutants at the NH_2-terminal phosphorylation sites[31], T53A, T58A, S71A, and one compound mutant, T53A-T58A-S71A, were generated and expressed in COS-7 cells, IL18-induced ERK1/2 phosphorylation declined substantially in T53A and T53A-T58A-S71A NCC-transfected COS-7 cells but not in those transfected with T58A or S71A (**Fig. 4g**), supporting a prominent role of the NH_2-terminal Thr^{53} of NCC in mediating IL18 signaling. The expression of several known NCC mutants identified in human subjects with Gitelman syndrome, including G439S, S475C, E121D, and Q1030R, of which had impaired thiazide-sensitive Na^+ uptake or cell membrane targeting[35,36], tested further the role of

IL18 in NCC activation. WT and G439S-transfected COS-7 cells had comparable IL18-induced p-ERK1/2, while S475C- and E121D-transfected cells had enhanced IL18-induced p-ERK1/2. Q1030R-transfected cells had blocked IL18-induced p-ERK1/2 (**Fig. 4h**), consistent with their corresponding cell membrane targeting profiles[35,36]. Immunoblot analysis using anti-p-NCC polyclonal antibody[37] on both whole cell lysate and cell membrane preparation from NCC- or vector-transfected COS-7 cells demonstrated functional NCC on COS-7 plasma membrane. P-NCC localized in cell membrane and whole cell lysate in NCC-transfected COS-7 cells after IL18 stimulation (**Fig. 4i**). NCC-transfected COS-7 cells elaborated IL6 after stimulation with IL18 with or without IL12 for 2 days, consistent with the cell signaling data presented in **Fig. 4f-4i**. In contrast, vector-transfected COS-7 cells did not release IL6 after IL18 treatment alone, and significantly less IL6 ($P < 0.001$) than did NCC-transfected cells after stimulation with both IL18 and IL12 (**Fig. 4j**, left). IL18-induced NCC phosphorylation, downstream signaling, and cytokine production did not require IL18r nor association with IL18r accessory protein (IL18rap). In NCC-transfected COS-7 cells, which do not express IL18r, co-transfection of Flag-tagged mouse IL18rap in pcDNA3.1 followed by immunoprecipitation with an anti-Flag antibody did not detect an association between NCC and IL18rap with or without IL18 treatment (**Supplementary Fig. 10**). The adoption of a previously established FlpIn-293 cell line that does not express IL18r (data not shown) but expresses a full-length NCC cDNA under a tetracycline-inducible promoter allowed for exploration of IL18 activity on NCC in other mammalian cells[37]. Active IL18, but not heat-inactivated IL18, induced both NCC expression and phosphorylation in FlpIn-293 cells exposed to tetracycline, as detected by immunoblot

(**Fig. 4j**, right two panels). In the kidney, NCC localizes primarily in distal tubular epithelial cells[38] and contributes to NaCl reuptake. Yet, tubular epithelial cells, glomerular parietal cells, mesangial cells, and endothelial cells can express IL18r[39], an important participant in glomerulonephritis, by regulating inflammatory cell infiltration, IgG and complement deposition, and inflammatory cytokine production[12,40]. NCC and IL18r therefore have distinct roles in the kidney.

This study demonstrated that IL18r and NCC coordinately participate in atherosclerosis (**Fig. 3a-3f, Supplementary Fig. 5a/5b**), and that these IL18-binding proteins colocalize in vascular SMCs, ECs, and macrophages (**Fig. 2b-2d, Supplementary Fig. 2**). IL18r and NCC may mediate IL18 signaling independently (**Fig. 2h**, **Fig. 4**)[16] or as a complex (**Fig. 2d/2g**), although informatic searches did not reveal sequence similarity between the intracellular domains of NCC and those of conventional cytokine receptors (data not shown). IL18-mediated NCC activation may also activate downstream cell signaling *via* increased cell volume or changes in intracellular Cl^- concentrations (**Supplementary Fig. 9**)[31,32]. Yet, this study does not exclude the involvement of additional molecules, either cell membrane proteins or extracellular soluble proteins that may participate in IL18 and NCC interaction. IL18 may contribute to atherogenesis in part by activating macrophages (**Fig. 4c/4d**), T cells (**Fig. 3g**), and possibly other inflammatory cells, such as mast cells and neutrophils to produce IFN-γ, IL6, IL18, and other untested inflammatory cytokines. The NCC activity in ion flux in the kidney may have negligible influence on atherogenesis, as shown in our BMT experiments presented in **Fig. 3a-3f** and **Supplementary Fig. 7**. Other organs under

inflammatory conditions may highly express NCC, which alongside IL18r, may mediate several important IL18 activities implicated in atherogenesis.

Method

Methods and any associated references are available on-line.

Acknowledgments

This study is supported by grants from the National Heart, Lung, and Blood Institute (HL60942, HL81090, HL88547, to GPS; HL34636, HL80472, to PL), and the American Heart Association Established Investigator Award (0840118N to GPS).

Author contributions

J.W. and C.S. performed most of the experiments. N.G. completed the original IL18 and IL18r mutant mouse analysis. C.L., M.L., M.A.S., A.H., Y.Z., H.C., J.Z., X.C., Q.K. performed RT-PCR, lesion analysis, cell culture, and plasma ELISA. J.L. helped with the NCC cDNA cloning. G.K.S. performed immunostaining. X.C., M.K., T.M., and P.L. helped with experimental design, writing, and data interpretation. M.J. and G.E.S. provided the NCC mutant mice. S.R., C.L.Y., and D.H.E. provided the NCC monoclonal antibody and performed the 293 cell experiments. S.J. and R.B. made the human NCC mutant constructs. P.J. measured plasma Mg and K. G.-P.S. designed and performed the experiments and wrote the manuscript.

References

1. Dinarello, C.A. IL-18: A TH1-inducing, proinflammatory cytokine and new member of the IL-1 family. *J. Allergy Clin. Immunol.* **103,** 11-24 (1999).
2. Yoshimoto, T. *et al.* IL-12 up-regulates IL-18 receptor expression on T cells, Th1 cells, and B cells: synergism with IL-18 for IFN-gamma production. *J. Immunol.* **161,** 3400-3407 (1998).
3. Elhage, R. *et al.* Reduced atherosclerosis in interleukin-18 deficient apolipoprotein E-knockout mice. *Cardiovasc. Res.* **59,** 234-240 (2003).
4. Mallat, Z*., et al.* Interleukin-18/interleukin-18 binding protein signaling modulates atherosclerotic lesion development and stability. *Circ Res* **89**, E41-45 (2001).

5. Gamba, G. *et al.* Molecular cloning, primary structure, and characterization of two members of the mammalian electroneutral sodium-(potassium)-chloride cotransporter family expressed in kidney. *J. Biol. Chem.* **269,** 17713-17722 (1994).
6. Okamura, H., Kashiwamura, S., Tsutsui, H., Yoshimoto, T., & Nakanishi, K. Regulation of interferon-gamma production by IL-12 and IL-18. *Curr. Opin. Immunol.* **10,** 259-264 (1998).
7. Konishi, H. *et al.* IL-18 contributes to the spontaneous development of atopic dermatitis-like inflammatory skin lesion independently of IgE/stat6 under specific pathogen-free conditions. *Proc. Natl. Acad. Sci. USA* **99,** 11340-11345 (2002).
8. French, A.R., Holroyd, E.B., Yang, L., Kim, S., & Yokoyama, W.M. IL-18 acts synergistically with IL-15 in stimulating natural killer cell proliferation. *Cytokine* **35,** 229-234 (2006).
9. Netea, M.G. *et al.* Deficiency of interleukin-18 in mice leads to hyperphagia, obesity and insulin resistance. *Nat. Med.* **12,** 650-656 (2006).
10. Sugiyama, M. *et al.* Deletion of IL-18 receptor ameliorates renal injury in bovine serum albumin-induced glomerulonephritis. *Clin. Immunol.* **128,** 103-108 (2008).
11. Gutcher, I., Urich, E., Wolter, K., Prinz, M., & Becher, B. Interleukin 18-independent engagement of interleukin 18 receptor-alpha is required for autoimmune inflammation. *Nat. Immunol.* **7,** 946-953 (2006).
12. Mallat, Z. *et al.* Expression of interleukin-18 in human atherosclerotic plaques and relation to plaque instability. *Circulation* **104,** 1598-1603 (2001).
13. Gerdes, N. *et al.* Expression of interleukin (IL)-18 and functional IL-18 receptor on human vascular endothelial cells, smooth muscle cells, and macrophages: implications for atherogenesis. *J. Exp. Med.* **195,** 245-257 (2002).
14. Whitman, S.C., Ravisankar, P., & Daugherty, A. Interleukin-18 enhances atherosclerosis in apolipoprotein E(–/–) mice through release of interferon-gamma. *Circ. Res.* **90,** E34-E38 (2002).
15. Tenger, C., Sundborger, A., Jawien, J., & Zhou, X. IL-18 accelerates atherosclerosis accompanied by elevation of IFN-gamma and CXCL16 expression independently of T cells. *Arterioscler. Thromb. Vasc. Biol.* **25,** 791-796 (2005).
16. Torigoe, K. *et al.* Purification and characterization of the human interleukin-18 receptor. *J. Biol. Chem.* **272,** 25737-25742 (1997).
17. Hoshino, K. *et al.* Cutting edge: generation of IL-18 receptor-deficient mice: evidence for IL-1 receptor-related protein as an essential IL-18 binding receptor. *J. Immunol.* **162,** 5041-5044 (1999).
18. Kunchaparty, S. *et al.* Defective processing and expression of thiazide-sensitive Na-Cl cotransporter as a cause of Gitelman's syndrome. *Am. J. Physiol.* **277,** F643-F649 (1999).
19. Gamba, G. *et al.* Primary structure and functional expression of a cDNA encoding the thiazide-sensitive, electroneutral sodium-chloride cotransporter. *Proc. Natl. Acad. Sci. USA* **90,** 2749-2753 (1993).
20. Schultheis, P.J. *et al.* Phenotype resembling Gitelman's syndrome in mice lacking the apical Na+-Cl- cotransporter of the distal convoluted tubule. *J. Biol. Chem.* **273,** 29150-29155 (1998).
21. Gjata, M., Tase, M., Gjata, A., & Gjergji, Zh. Gitelman's syndrome (familial hypokalemia-hypomagnesemia). *Hippokratia.* **11,** 150-153 (2007).

22. Morris, R.G., Hoorn, E.J., & Knepper, M.A. Hypokalemia in a mouse model of Gitelman's syndrome. *Am. J. Physiol. Renal Physiol.* **290,** F1416-F1420 (2006).
23. Tzanakis, I. *et al.* Intra- and extracellular magnesium levels and atheromatosis in haemodialysis patients. *Magnes. Res.* **17,** 102-108 (2004).
24. Hulthe, J. *et al.* Plasma interleukin (IL)-18 concentrations is elevated in patients with previous myocardial infarction and related to severity of coronary atherosclerosis independently of C-reactive protein and IL-6. *Atherosclerosis* **188,** 450-454 (2006).
25. Blankenberg, S. *et al.* Interleukin-18 is a strong predictor of cardiovascular death in stable and unstable angina. *Circulation* **106,** 24-30 (2002).
26. Lauwerys, B.R., Renauld, J.C., & Houssiau, F.A. Synergistic proliferation and activation of natural killer cells by interleukin 12 and interleukin 18. *Cytokine* **11,** 822-830 (1999).
27. Brunet, A. *et al.* Nuclear translocation of p42/p44 mitogen-activated protein kinase is required for growth factor-induced gene expression and cell cycle entry. *EMBO J.* **18,** 664-674 (1999).
28. Ono, K., & Han, J. The p38 signal transduction pathway: activation and function. *Cell Signal.* **12,** 1-13 (2000).
29. Hossain Khan, M.Z.*, et al.* Phosphorylation of Na-Cl cotransporter by OSR1 and SPAK kinases regulates its ubiquitination. *Biochem Biophys Res Commun* **425**, 456-461 (2012).
30. Yang, S.S. *et al.* Generation and analysis of the thiazide-sensitive Na+ -Cl- cotransporter (Ncc/Slc12a3) Ser707X knockin mouse as a model of Gitelman syndrome. *Hum. Mutat.* **31,** 1304-1315 (2010).
31. Pacheco-Alvarez, D. *et al.* The Na+:Cl- cotransporter is activated and phosphorylated at the amino-terminal domain upon intracellular chloride depletion. *J. Biol. Chem.* **281,** 28755-28763 (2006).
32. Rozansky, D.J. *et al.* Aldosterone mediates activation of the thiazide-sensitive Na-Cl cotransporter through an SGK1 and WNK4 signaling pathway. *J. Clin. Invest.* **119,** 2601-2612 (2009).
33. Griffon, N., Jeanneteau, F., Prieur, F., Diaz, J., & Sokoloff, P. CLIC6, a member of the intracellular chloride channel family, interacts with dopamine D(2)-like receptors. *Mol. Brain Res.* **117,** 47-57 (2003).
34. Heim, M.H. The Jak-STAT pathway: cytokine signalling from the receptor to the nucleus. *J. Recept. Signal. Transduct. Res.* **19,** 75-120 (1999).
35. De Jong, J.C.*, et al.* Functional expression of mutations in the human NaCl cotransporter: evidence for impaired routing mechanisms in Gitelman's syndrome. *J Am Soc Nephrol* **13**, 1442-1448 (2002).
36. Glaudemans, B.*, et al.* Novel NCC mutants and functional analysis in a new cohort of patients with Gitelman syndrome. *Eur J Hum Genet* **20**, 263-270 (2012).
37. Hoorn, E.J. *et al.* The calcineurin inhibitor tacrolimus activates the renal sodium chloride cotransporter to cause hypertension. *Nat. Med.* **17,** 1304-1309 (2011).
38. Reilly, R.F., & Ellison, D.H. Mammalian distal tubule: physiology, pathophysiology, and molecular anatomy. *Physiol. Rev.* **80,** 277-313 (2000).
39. Miyauchi, K., Takiyama, Y., Honjyo, J., Tateno, M., & Haneda, M. Upregulated IL-18 expression in type 2 diabetic subjects with nephropathy: TGF-beta1 enhanced IL-

18 expression in human renal proximal tubular epithelial cells. *Diabetes Res. Clin. Pract.* **83,** 190-199 (2009).
40. Kinoshita, K. *et al.* Blockade of IL-18 receptor signaling delays the onset of autoimmune disease in MRL-Faslpr mice. *J. Immunol.* **173,** 5312-5318 (2004).

Figure legends

Figure 1. Identification of alternative IL18-binding proteins. **a.** Aortic root lesion intima, Mac-3^+ macrophage, $CD4^+$ T cell, and α-actin–positive SMC areas in *Apoe*$^{-/-}$*Il18r*$^{-/-}$ and *Apoe*$^{-/-}$ mice. n=7-10 per group. **b.** FACS of ECs from *Apoe*$^{-/-}$*Il18r*$^{-/-}$ and *Apoe*$^{-/-}$ mice after binding with biotin-IL18 with and without excessive non-labeled IL18, followed by incubation with PE-streptavidin. **c.** P-tyrosine immunoblot in ECs treated with and without IL18 or heat-inactivated IL18 for 30 minutes. Actin, loading control. **d.** IL18-binding protein identification in ECs from *Apoe*$^{-/-}$*Il18r*$^{-/-}$ mice. SDS-PAGE silver staining detected IL18-bound proteins in three sequential elutes from anti-IL18 antibody-bound protein-A agarose beads pre-incubated with cell lysates from ECs treated with or without IL18.

Figure 2. Na-Cl co-transporter expression and characterization. **a.** Immunostaining of NCC in normal human (bar: 1000 μm) and mouse aortas (bar: 50 μm). **b.** Immunostaining of NCC, IL18r, and $CD68^+$ macrophages in human atherosclerotic lesions. Negative controls rabbit and mouse (not shown) IgG. Bar: 500 μm. **c.** Immunostaining of NCC in lesions from *Apoe*$^{-/-}$ mice. Macrophage, SMC, and EC areas were framed. Negative controls used lesions from *Apoe*$^{-/-}$*Ncc*$^{-/-}$ mice. Bar: 200 μm, insert bar: 50 μm. **d.** Immunofluorescent staining of NCC and IL18r in macrophages, SMCs, and ECs from lesions from *Apoe*$^{-/-}$ mice. Bar: 50 μm. **e.** RT-PCR and immunostaining to

detect NCC in macrophages (bar: 50 μm) and T cells (bar: 20 μm) from *Apoe*$^{-/-}$ mice. Immunostaining negative controls used macrophages from *Apoe*$^{-/-}$*Ncc*$^{-/-}$ mice. **f.** Immunoblots to detect NCC in cytokine-induced mouse ECs and SMCs. NCC doublets are indicated. Positive control used NCC-transfected COS-7 cell lysate. **g.** IL18r immunoprecipitation followed by NCC immunoblot to detect NCC-IL18r complexes in macrophages from *Apoe*$^{-/-}$ mice. Negative control used macrophages from *Apoe*$^{-/-}$*Ncc*$^{-/-}$ mice. **h.** FACS to detect biotin-IL18 and heated biotin-IL18 binding to differently transfected COS-7 cells; Scatchard plot of FITC-IL18 binding affinity on NCC-transfected COS-7 cells, and p-tyrosine immunoblot in NCC- or vector-transfected COS-7 cells treated with different treatments. Actin, protein loading. Data in panels **e** and **h** are mean ± SEM from three to six independent experiments.

Figure 3. IL18r and NCC function in atherosclerosis. Aortic root lesion intima area (**a**), thoracic-abdominal aorta oil-red O staining with representative images shown to the right, bar: 1 cm (**b**), aortic root lesion Mac-3^{+} macrophages, CD4^{+} T cell numbers, and MHC class-II-positive areas (**c**), lesion SMC content (**d**), aortic root oil-red O positive areas (**e**), and plasma IFN-γ, IL6, and IL18 levels (**f**) in *Apoe*$^{-/-}$, *Apoe*$^{-/-}$*Ncc*$^{-/-}$, *Apoe*$^{-/-}$*Il18r*$^{-/-}$ and *Apoe*$^{-/-}$*Ncc*$^{-/-}$*Il18r*$^{-/-}$ mice and in *Apoe*$^{-/-}$*Ncc*$^{-/-}$*Il18r*$^{-/-}$ mice receiving BMT from *Apoe*$^{-/-}$, *Apoe*$^{-/-}$*Il18r*$^{-/-}$ and *Apoe*$^{-/-}$*Ncc*$^{-/-}$*Il18r*$^{-/-}$ mice, after consuming a Western diet for 12 weeks, n=7-11 per group. ELISA determined media IFN-γ and IL6 levels in CD4^{+} T cells from different mice after stimulation without (control) or with IL18 and IL12 (**g**). Data in panel **g** are mean ± SEM from three independent experiments.

Figure 4. NCC binding, signaling, and cytokine and chemokine production in macrophages, COS-7 cells, and FlpIn-293 cells. **a.** Scatchard plot of FITC-IL18 binding affinity on macrophages from *Apoe*$^{-/-}$*Il18r*$^{-/-}$ mice. **b.** p-ERK1/2 and p-p38 immunoblots in macrophages from different mice treated with and without IL18. Total ERK1/2, loading control. **c.** ELISA determined medium INF-γ and MCP-1 in IL18-treated and untreated macrophages from different mice. **d.** ELISA determined media IL6 in macrophages from different mice and treated with and without IL8 and hydrochlorothiazide. p-EKR1/2 immunoblot of macrophages from *Apoe*$^{-/-}$ and *Apoe*$^{-/-}$ *Il18r*$^{-/-}$ mice are shown to the right. **e.** p-SPAK immunoblot in macrophages from different mice as indicated. **f.** p-STAT3, p-p38, and p38 immunoblots of cell lysates from NCC- or vector-transfected COS-7 cells and stimulated with IL18, or IL18 with IL12. **g/h.** p-ERK1/2 immunoblot of COS-7 cells transfected with indicated cDNA construct in pcDNA31 (**g**) or pCI-neo (**h**) and stimulated with or without IL18 for 15 minutes. **i.** Immunoblots to detect p-NCC in membrane fraction or total cell lysate from vector- or NCC-transfected COS-7 cells and stimulated with or without IL18. **j.** Medium IL6 ELISA in COS-7 cells with different transfections and stimulations; immunoblots to detect total and p-NCC in FlpIn-293 cells induced with or without tetracycline, IL18, or heat-inactivated IL18. Immunoblot signal density quantifications are shown to the right. Data in panels **a**, **c**, **d,** and **j** are mean ± SEM from three to six independent experiments.

On-line methods

Generation of *Apoe*$^{-/-}$*Il18r*$^{-/-}$, *Apoe*$^{-/-}$*Ncc*$^{-/-}$, and *Apoe*$^{-/-}$*Ncc*$^{-/-}$*Il18r*$^{-/-}$ mice, and atherosclerotic lesion characterization. *Apoe*$^{-/-}$ mice (C57BL/6, N12, The Jackson Laboratory, Bar Harbor, ME), *Il18r*$^{-/-}$ (C57BL/6, N10, The Jackson Laboratory) and *Ncc*$^{-/-}$ mice (C57BL/6/129S background)[20] were crossbred to generate *Apoe*$^{-/-}$, *Apoe*$^{-/-}$*Il18r*$^{-/-}$, *Apoe*$^{-/-}$*Ncc*$^{-/-}$, and *Apoe*$^{-/-}$*Ncc*$^{-/-}$*Il18r*$^{-/-}$ mice in C57BL/6/129S mixed background littermates. All four groups of mice had the same genetic background as confirmed by genome scanning performed by the Jackson Laboratory. In this study, we used 7 to 11 mice per experimental group based on the availability from the crossbreeding. Male 6-week-old mice consumed a Western diet (Research Diet, New Brunswick, NJ) for 12 weeks to develop atherosclerosis. Before harvesting mouse aortas, we collected plasma samples for plasma cytokine measurement (IL6 and IFN-γ) with ELISA kits according to the manufacturer's instructions (R&D Systems, Minneapolis, MN). To characterize mouse atherosclerotic lesions, we embedded aortic root in OCT compound (Sakura Finetek USA, Inc., Torrance, CA) and prepared seven slides that each contained three 6-μm frozen serial sections through the aortic sinus. The lesions in the root of the aorta beneath all three-valve leaflets near the ostia of the coronary arteries were analyzed. To characterize atherosclerotic lesion composition, we stained frozen sections for macrophages (Mac-3, 1:900, clone M3/84), $CD4^+$ T cells (CD4, 1:90, clone OX-35), MHC class-II (1:150, clone M5/114.15.2) (Pharmingen, San Diego, CA), and SMCs (α-actin, 1:750, #SAB2500963, Sigma, St. Louis, MO)[41]. We performed each staining on a single slide from the same level of aortic root for all experimental and control mice. Computer-assisted analysis (Image-Pro Plus) served to determine the lesion size, as well as lipid deposition and areas for specific cell types in the cross-sections from aortic roots from the same experiment by the same observer to minimize variations. All measurements were performed by manual selection of stained pixel threshold and presented as percent of positive (stained) area to the entire intimal area. $CD4^+$ T cells were counted and presented as number of T cells per square millimeter. Thoracic-abdominal aortas were used for en-face preparation and oil-red O staining to detect lipid deposition[41,42]. Plasma IL6, IFN-γ, IL18 (eBioscience, San Diego, CA), cholesterol, triglyceride, and high-density lipoproteins (Fisher Scientific, Pittsburg, PA) were determined by ELISA according to the manufacturers. Plasma Mg^{2+} and K^+ levels were determined using the cobas c501 clinical chemistry analyzer using ion selective electrodes for potassium testing and the colorimetric MG2 assay for magnesium testing (Roche Diagnostics, Indianapolis, IN). Specimens with gross hemolysis were excluded from testing. Investigators were blinded during mouse harvesting and lesion characterization. All animal procedures conformed to the Guide for the Care and Use of Laboratory Animals published by the U.S. National Institutes of Health and were approved by the Harvard Medical School Standing Committee on Animals (protocol #03759).

Bone marrow transplantation. Male 8-week-old *Apoe*$^{-/-}$*Ncc*$^{-/-}$*Il18r*$^{-/-}$ mice were subjected to 1000 rad of total body irradiation, followed by reconstitution of 2×10^6 bone marrow cells from *Apoe*$^{-/-}$, *Apoe*$^{-/-}$*Il18r*$^{-/-}$, and *Apoe*$^{-/-}$*Ncc*$^{-/-}$*Il18r*$^{-/-}$ mice via tail-vein injection. All animals were allowed to recover for 4 weeks on a chow diet after BMT.

Recipient mice then consumed an atherogenic diet for 12 weeks to develop atherosclerosis.

Thiazide diuretics and IL18 treatments. Male 8-week-old *Apoe*$^{-/-}$ and *Apoe*$^{-/-}$*Il18r*$^{-/-}$ mice received hydrochlorothiazide (25 mg/L in drinking water, Sigma) while consuming an atherogenic diet for 12 weeks according to a previously established protocol[43]. Male 8-week-old *Apoe*$^{-/-}$ and *Apoe*$^{-/-}$*Ncc*$^{-/-}$*Il18r*$^{-/-}$ mice received daily intraperitoneal injections of recombinant mouse IL18 (30 ng/gram body weight in 200 μL saline, MBL International, Woburn, MA) or saline alone for four weeks as described[14].

Detections of NCC and IL18r in atherosclerotic lesions, kidney, macrophages, and T cells. Frozen sections from human normal carotid artery, carotid atherosclerotic lesions, and fatty streaks were immunostained with rabbit anti-human/mouse NCC polyclonal (1:60, #AB3553, Millipore, Billerica, MA), mouse anti-human IL18r monoclonal (1:100, clone 70625, R&D Systems), mouse anti-CD68 monoclonal (1:900, clone KP1, Dako, Carpinteria, CA) antibodies, mouse IgG1 (1:50, clone MOPC-31C, Becton Dickinson, Franklin Lakes, NJ) and rabbit IgG (1:60, #I5006, Sigma). Frozen sections of mouse kidney, normal mouse aorta, and atherosclerotic lesions from *Apoe*$^{-/-}$ and *Apoe*$^{-/-}$*Ncc*$^{-/-}$ mice were immunostained with anti-mouse NCC polyclonal antibodies (1:250) from Millipore (Billerica, MA) or those previously described[18,44]. To detect NCC expression in macrophages, cells were cultured on a 4-well chamber slide. After stimulation with or without IL18, the slide was fixed with 10% formalin, and immunostained with anti-mouse NCC polyclonal antibody (1:250)[18,44]. T cells were treated with IL18, fixed with 10% formalin, and immunostained with the same antibody (1:250) in a test tube followed by photograph. To colocalize NCC and IL18r in mouse atherosclerotic lesions, we applied rabbit anti-NCC antibody (1:60, Millipore) after a 1-hour block in PBS, supplemented with 10% normal goat serum and 2% BSA (bovine serum albumin) for overnight incubation at 4°C followed by goat anti-rabbit Alexa Fluor 555 (red, 1:500, #A-21428, Invitrogen, Carlsbad, CA). After extensive washing in PBS, mouse anti-IL18r antibodies were applied (1:50, R&D Systems) for 1.5 hours, followed by goat anti-mouse Alexa Fluor 488 (green, 1:300, #A-31561, Invitrogen). After nuclei staining with DAPI, slides were cover-slipped with Fluorescent Mounting Medium (DAKO) and analyzed by Inverted Nikon eclipse TE2000-U microscope.

Isolation of mouse ECs, SMCs, CD4$^+$ T cells, and macrophages. Primary ECs were isolated using positive immuno-selection, as previously described[45]. Briefly, a mouse lung was minced and incubated with 2 mg/ml collagenase type I (Worthington Biochemical Corp., Lakewood, NJ) at 37 °C in DMEM for 1 hour, followed by incubation with anti-mouse CD31 (clone 390, Pharmingen)-coated DYNAL® Magnetic Beads (Invitrogen) for 10 minutes. Cells were separated with a magnetic separator and cultured on 0.1% gelatin–coated plates. After the cells reached confluence, a second purification was performed with rat anti-mouse CD102 antibody (clone 3C4(mIC2/4), Pharmingen). EC purity was examined by flow cytometry with anti-CD31 antibody. Mouse aortic SMCs were isolated by collagenase type II (Worthington) digestion of aorta for 10 minutes, and the adventitia and endothelia were removed with abrasion, followed by digestion with collagenase types I and III (Worthington) for 60 minutes[41]. Cells were

then plated on a fibronectin-coated plate. SMC identity was verified by immunostaining for □-actin. $CD4^+$ T cells were isolated from mouse spleen, as we reported previously[46]. Briefly, crude total T cells were separated from splenocytes using a nylon-wool column (Polysciences, Inc., Warrington, PA). Crude preparation was used to deplete antigen-presenting cells and $CD8^+$ T cells by two rounds of incubation with $I\text{-}A^b$ and CD8 monoclonal antibodies (clone AF6-120.1 and clone 53-6.7, Pharmingen) for 30 minutes at 4 ºC, followed by lysis with low-tox complement (Accurate Chemical and Science Corp., Westbury, NY) at 37 ºC for 30 minutes. To obtain macrophages, mice were intraperitoneally injected with 3% thioglycollate (Sigma). After 72 hours, peritoneal cells were collected and cultured with RPMI 1640 in a plate overnight. After suspended cells were removed, macrophages adhered to the plate were used for further experiments.

IL18-binding Na-Cl co-transporter identification. An immunoprecipitation kit (Promega, Madison, WI) was used to isolate IL18 binding proteins. Briefly, ECs from *Il18r*$^{-/-}$ mice were incubated with recombinant mouse IL18 (PeproTech, Inc., Rocky Hill, NJ, 50 ng/ml) for 15 minutes at 37 ºC, washed with ice-cold PBS, lysed in a lysis buffer from the immunoprecipitation kit, and centrifuged at 14000 rpm for 15 minutes. The supernatant was passed through an IL18 polyclonal antibody (#5180R, BioVision, Inc., Milpitas, CA) pre-coated protein A agarose (Invitrogen) column, followed by extensive washes. Bound proteins were eluted according to the manufacturer's instructions, and separated on an 8% SDS-PAGE. Silver staining displayed two bands of approximately 80-kDa and 125-kDa, which were removed and analyzed with mass spectrometry (Brigham and Women's Hospital Core Facility).

Cloning and expression of mouse and human wild-type and mutant NCC and IL18rap. A full-length wild-type (WT) mouse NCC cDNA fragment was amplified from mouse EC RNA using RT-PCR, with a forward primer covering the start codon and a reverse primer covering the stop codon (NM_019415). Full-length cDNA subcloned into pcDNA3.1 (Invitrogen). NCC/pcDNA3.1 and empty vector were used for COS-7 cell transfection with lipofectamine (Invitrogen). Site-direct mutagenesis was performed to replace three phosphorylation sites — Thr^{53}, Thr^{58}, and Ser^{71} — or all three amino acids together located at the NH_2-terminus of NCC with alanine, using the original NCC/pcDNA3.1 as a template (GenScript USA Inc., Piscataway, NJ). A full-length mouse IL18rap cDNA with a Flag tag at the COOH-terminus was subcloned to the same pcDNA3.1 expression vector (Bioclone, Inc., San Diego, CA). Human NCC cDNA was subcloned into the pCI-neo (Promega) and site-direct mutagenesis was used to generate G439S, S475C, E121D, and Q1030R mutants, followed by lipofectamine-mediated transfection into COS-7 cells.

Flow cytometry. Recombinant mouse IL18 was biotinylated with an EZ-link biotinylation kit (Pierce, Rockford, IL) according to the manufacturer's instructions. ECs isolated from *Apoe*$^{-/-}$ and *Apoe*$^{-/-}$*Il18r*$^{-/-}$ mice or COS-7 cells transfected with NCC/pcDNA 3.1 were incubated with 10 ng/ml biotin-IL18, in the absence or presence of unlabeled IL18, for 10 minutes or 30 minutes at 37ºC, followed by incubation with 1:100 diluted PE-conjugated streptavidin (#562284, Pharmingen). After three washes, cells were subjected to flow cytometric analysis.

Immunoblot, RT-PCR, ELISA, and cell volume measurement. To detect protein tyrosine phosphorylations, mouse ECs, wild-type or mutant NCC-transfected COS-7 cells, or macrophages were starved overnight and then treated with or without IL18, heat-inactivated IL18 (50~100 ng/ml), or IL12 (10 ng/ml) (PeproTech) for 15 to 30 minutes. Equal amounts of protein from each cell-type preparation were separated by SDS-PAGE, blotted, and detected with different antibodies, including p-tyrosine (1:1000, #309302, BioLegend, San Diego, CA), p-p38 MAPK (Thr^{180}/Tyr^{182}, #4511, 1:1000), and p-ERK (p-p44/42 MAPK, #9107, 1:1000); p-STAT3 (Ser727, #9136, 1:1000) (Cell Signaling Technology, Inc., Danvers, MA); p-NCC (1:500)[37], p-SPAK (1:1000, obtained from the Division of Signal Transduction Therapy Unit at the University of Dundee), and β-actin (1:3000, #A5441, Sigma). To detect NCC activation in COS-7 cells, we transfected COS-7 cells with pcDNA3.1 or NCC/pcDNA3.1, followed by IL18 (100 ng/ml) treatment for 15 minutes. Cell membrane fraction and cytosolic fraction were extracted according to the manufacturer's instructions (Fraction PREP cell fractionation kit, BioVision). Equal amounts of protein were separated by SDS-PAGE and detected with phospho-NCC[37] and total NCC (Millipore) polyclonal antibodies (1:1000). Transfected COS-7 cells were photographed, and cell volumes were measured using computer-assisted analysis (Image-Pro Plus). To express NCC in HEK293 cells, we used the Flp-In T-Rex mammalian expression system (Invitrogen), which permitted expression of NCC under the control of a tetracycline-inducible promoter, and allowed NCC to process normally by glycosylation and phosphorylation[37]. FlpIn-293 cells were maintained in a high-glucose DMEM containing 10% FBS, 200 μg/ml hygromycin, 15 μg/ml blasticidin, and penicillin/streptomycin. NCC induction was confirmed by incubating the cells with or without tetracycline (1 μg/ml). To stimulate NCC expression and phosphorylation, we pre-treated FlpIn-293 cells with or without tetracycline overnight[37] and then with or without IL18 (100 ng/ml) for another overnight, followed by cell lysis and immunoblotting using anti-total-NCC[44] or anti-phospho-NCC[37] rabbit polyclonal antibodies.

To detect NCC expression in mouse SMCs and ECs, cells were starved overnight and then stimulated with IL18 (50 ng/ml), IL1β (10 ng/ml), or TNF-α (10 ng/ml) (PeproTech) for 2 days. Immunoblot was used to detect NCC expression in these cells using rabbit anti-mouse NCC polyclonal antibody (1:1000, Millipore).

To detect cytokine (IL6 and IFN-γ) and chemokine (MCP-1) expression in $CD4^+$ T cells, peritoneal macrophages, and COS-7 cells, cells were starved overnight and then stimulated with IL18 (50~100 ng/ml, MBL International), IL18 with IL12 (10 ng/ml, PeproTech), hydrochlorothiazide (200 μM, Sigma)[47], or TGF-β1 (10 ng/ml, R&D Systems) for 2 days. Macrophages were pre-incubated with IL1β and TNF-α for 2 days to induce NCC expression before other treatments. Cell culture media were collected to measure medium cytokines and chemokines with ELISA kits, according to the manufacturer's instructions (R&D Systems). Cells were collected for total RNA preparation and RT-PCR analysis (Bio-Rad, Hercules, CA) to detect IL6, IFN-γ, and MCP-1 mRNA levels.

NCC co-immunoprecipitation with IL18rap and IL18r. Flag-IL18rap and NCC plasmids were transfected into COS-7 cells with lipofectamine 2000 (Invitrogen). After

48 hours, cells were treated with or without IL18 (100 ng/ml) for 15 minutes and then lysed in a RIPA buffer containing 50 mM Tris, pH 7.4, 150 mM NaCl, 2 mM EDTA, 1% NP-40, 0.1% SDS, 5 μg/ml aprotinin, 5 μg/ml leupeptin, and 1 mM phenylmethylsulfonyl fluoride. To detect the protein expression, an equal amount of protein from each preparation was separated by SDS-PAGE, blotted, and detected with different antibodies, including Flag (1:1000, clone M2, Sigma), NCC (1:1000)[37], and β-actin (1:3000, Sigma). For immunoprecipitation, cell lysates were pre-cleared for 1 hour with protein A/G agarose (Santa Cruz Biotechnology Inc., Dallas, TX), followed by incubating overnight with 1 μg anti-Flag antibody (Sigma) and protein A/G agarose for an additional hour. Immunoprecipitates were then washed four times with 1 ml cell lysis buffer, followed by separation on 8% SDS-PAGE for immunoblot analysis with rabbit anti–mouse NCC polyclonal antibody (1:1000)[37].

To detect the interaction between NCC and IL18r, we used macrophages from *Apoe*$^{-/-}$ and *Apoe*$^{-/-}$*Ncc*$^{-/-}$ mice instead of transfecting NCC together with all three chains of IL18r to COS-7 cells, which may affect IL18r function. Macrophages were treated with and without IL18 for 30 min and cell lysates (300 μg per sample) were immunoprecipitated with rat anti-mouse IL18r monoclonal antibody (clone 112624, R&D Systems) followed by immunoblot with rabbit anti-NCC polyclonal antibody (Millipore) to detect NCC-IL18r complexes.

IL18 binding and Scatchard plot analysis. Mouse recombinant IL18 (PeproTech) was conjugated with FITC using a Sigma FITC conjugation kit. Briefly, IL18 was diluted at 5.0 mg/ml in 0.1 M carbonate-bicarbonate buffer, pH 9.0, and combined with 50 μl FITC solution with different dilutions (5:1, 10:1, 20:1), according to the manufacturer's instructions. Reaction was carried at room temperature under dark for 2 hours. FITC-conjugated IL18 was purified over a Sephadex G-25M column.

Binding assay was performed according to an established protocol from PerkinElmer, Inc. (DELFIA® Eu-Labled IL18). In brief, COS-7 cells or mouse peritoneal macrophages were resuspended in a buffer containing 20 mM HEPES and 10 mM EDTA, pH 7.5, and incubated at 4 ºC for 15 minutes. Cells were then homogenized and centrifuged at 28000 rpm, at 4 ºC for 30 minutes. Cell pellet was resuspended into a storage buffer containing 20 mM HEPES and 1 mM EDTA, pH 7.5, and rehomogenized with polytron PT3100 homogenizer. An equal amount of protein was incubated with FITC-IL18 in a binding buffer (50 mM Tris-HCL, 5 mM $MgCl_2$, 25 μM EDTA, 0.2% BSA) for 90 minutes at room temperature in an AcroWell^{TM} 96 Filter Plate (Pall Corp., Port Washington, NY). The plate was then washed four times with 50 mM Tris-HCl and 5 mM $MgCl_2$. The plate was read at 494 nm excitation and 518 nm emission. Scatchard analysis was performed using the Prism 3.02 software (GraphPad Software Inc., La Jolla, CA). To test FITC-IL18 binding affinity on NCC from COS-7 cells, which do not express IL18r (data not shown), we used NCC-transfected COS-7 cells. Empty vector-transfected COS-7 cells were used for background controls. To test FITC-IL18 binding affinity on macrophages, we used adhesion depletion-purified peritoneal macrophages from *Apoe*$^{-/-}$ *Il18r*$^{-/-}$ mice, and the same cells from *Apoe*$^{-/-}$*Ncc*$^{-/-}$*Il18r*$^{-/-}$ mice were used as background controls. Data were presented as the mean of three to five experiments.

Intracellular chloride measurements. To detect intracellular chloride concentration, COS-7 cells were transfected with pcDNA3.1 or NCC/pcDNA3.1 for 2 days. Intracellular chloride concentration was then monitored by a chloride-sensitive fluorescent dye, n-(ethoxycarbonylmethyl)-6-methoxyquinolinium (MQAE), as described[33]. Briefly, cells were first incubated with 10 mM MQAE in a loading buffer [DMEM, 0.1% BSA, 10 mM 4-(2-hydroxyethyl)-1-piperazine-ethanesulphonic acid (HEPES), pH 7.5] for 45 minutes at 37 °C. Cells were then washed with DMEM or with chloride-free medium (101 mM sodium gluconate, 5 mM potassium gluconate, 2 mM $MgSO_4$, 2 mM calcium acetate, 10 mM HEPES, pH 7.5, 10 mM glucose), and fluorescence was excited at 350 nm and detected at 460 nm. The time course of MQAE was monitored using a fluorescence spectrophotometer Wallac (Perkin Elmer) for 5 minutes, followed by the addition of NaCl (25 mM) for 5 minutes. Reduction of intracellular (efflux) chloride concentration is expected as an increase in fluorescence.

Statistical analysis. We used the non-parametric Mann-Whitney test followed by Bonferroni correction to examine the statistical significance between the groups, due to the relatively small sample sizes and often skewed distributions. $P < 0.05$ was considered statistically significant. All data were expressed as mean ± SEM. The availability and our prior experience, but not Power Calculation determined the number of mice in each experimental group. No data point was excluded.

References

41. Sukhova, G.K. *et al.* Deficiency of cathepsin S reduces atherosclerosis in LDL receptor-deficient mice. *J. Clin. Invest.* **111,** 897-906 (2003).
42. Mach, F., Schönbeck, U., Sukhova, G.K., Atkinson, E., & Libby, P. Reduction of atherosclerosis in mice by inhibition of CD40 signalling. *Nature* **394,** 200-203 (1998).
43. Zhang, M.Z*., et al.* Role of blood pressure and the renin-angiotensin system in development of diabetic nephropathy (DN) in eNOS-/- db/db mice. *Am J Physiol Renal Physiol* **302**, F433-438 (2012).
44. Bostanjoglo, M. *et al.* 11Beta-hydroxysteroid dehydrogenase, mineralocorticoid receptor, and thiazide-sensitive Na-Cl cotransporter expression by distal tubules. *J. Am. Soc. Nephrol.* **9,** 1347-1358 (1998).
45. Zhang, J. *et al.* Regulation of endothelial cell adhesion molecule expression by mast cells, macrophages, and neutrophils. *PLoS One.* **6,** e14525 (2011).
46. Shi, G.P. *et al.* Cathepsin S required for normal MHC class II peptide loading and germinal center development. *Immunity* **10,** 197-206 (1999).
47. Markadieu, N*., et al.* A primary culture of distal convoluted tubules expressing functional thiazide-sensitive NaCl transport. *Am J Physiol Renal Physiol* **303**, F886-892 (2012).

Type of file: figure
Label: 1
Filename: figure_1.tif

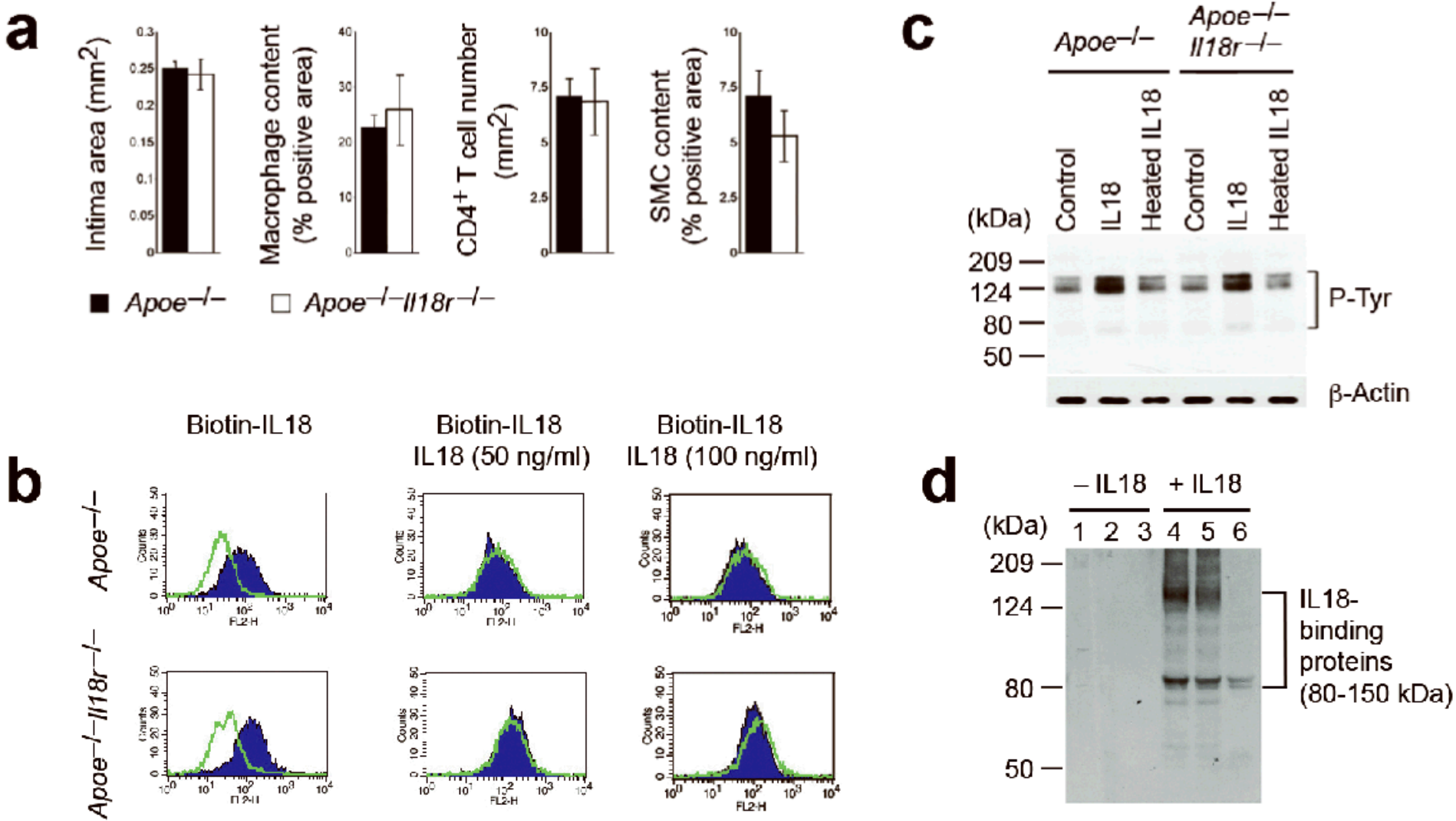
a
Intima area (mm2)
Macrophage content (% positive area)
CD4+ T cell number (mm2)
SMC content (% positive area)
Apoe−/−
Apoe−/−Il18r−/−
b
Biotin-IL18
Biotin-IL18 IL18 (50 ng/ml)
Biotin-IL18 IL18 (100 ng/ml)
Apoe−/−
Apoe−/−Il18r−/−
Counts
FL2-H
c
Apoe−/−
Apoe−/− Il18r−/−
Control
IL18
Heated IL18
(kDa)
209
124
80
50
P-Tyr
β-Actin
d
– IL18
+ IL18
(kDa)
1 2 3 4 5 6
209
124
80
50
IL18-binding proteins (80-150 kDa)

Type of file: figure
Label: 2
Filename: figure_2.tif

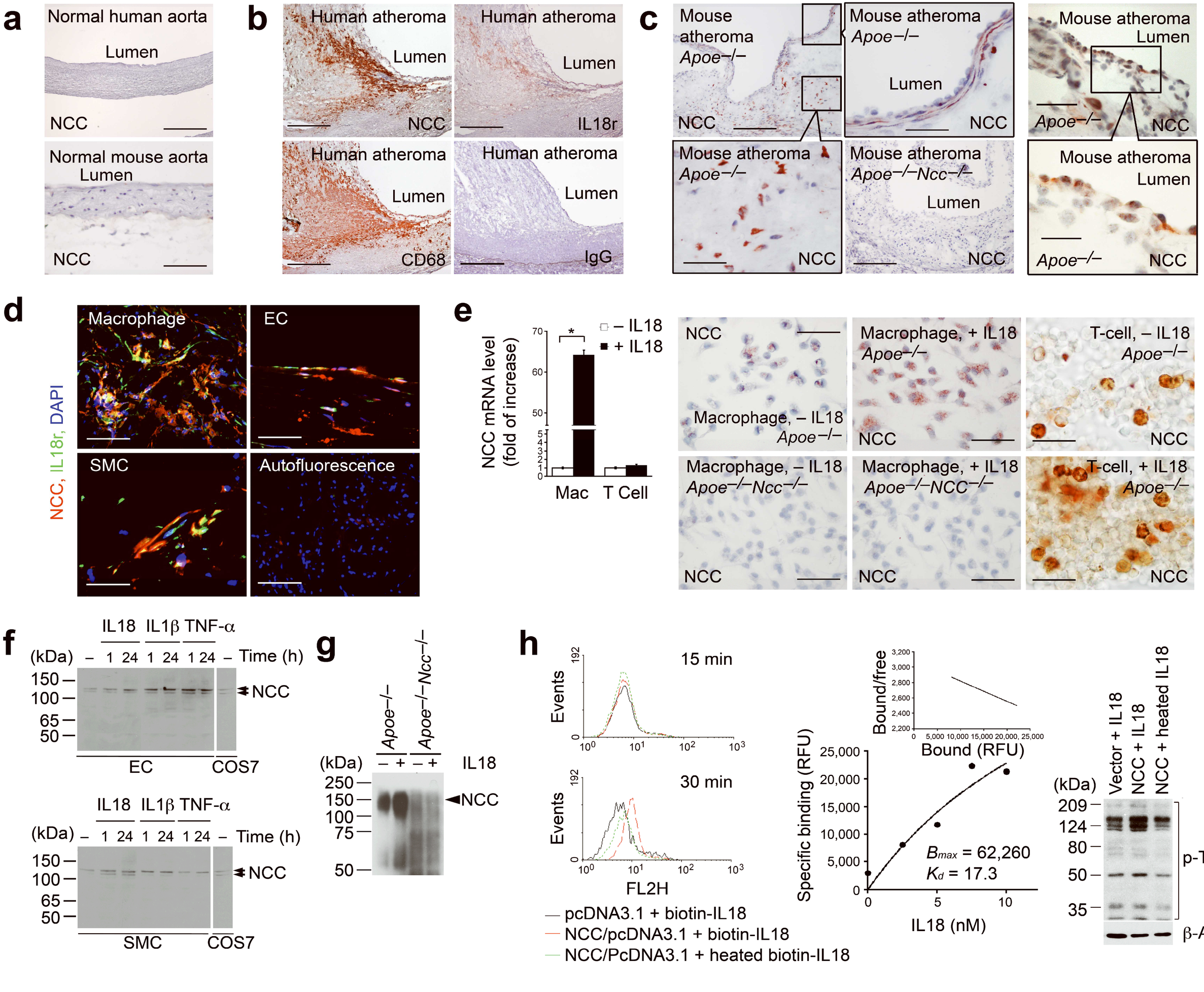
a
Normal human aorta
Lumen
NCC
Normal mouse aorta
Lumen
NCC
b
Human atheroma
Lumen
NCC
Human atheroma
Lumen
IL18r
Human atheroma
Lumen
CD68
Human atheroma
Lumen
IgG
c
Mouse atheroma Apoe−/−
NCC
Mouse atheroma Apoe−/−
Lumen
NCC
Mouse atheroma
Lumen
Apoe−/−
NCC
Mouse atheroma Apoe−/−
NCC
Mouse atheroma Apoe−/−Ncc−/−
Lumen
NCC
Mouse atheroma
Lumen
Apoe−/−
NCC
d
Macrophage
EC
SMC
Autofluorescence
NCC, IL18r, DAPI
e
NCC mRNA level (fold of increase)
70
60
50
5
4
3
2
1
0
*
– IL18
+ IL18
Mac
T Cell
NCC
Macrophage, – IL18 Apoe−/−
Macrophage, + IL18 Apoe−/−
NCC
T-cell, – IL18 Apoe−/−
NCC
Macrophage, – IL18 Apoe−/−Ncc−/−
NCC
Macrophage, + IL18 Apoe−/−NCC−/−
NCC
T-cell, + IL18 Apoe−/−
NCC
f
IL18 IL1β TNF-α
(kDa) – 1 24 1 24 1 24 – Time (h)
150
100
65
50
NCC
EC
COS7
IL18 IL1β TNF-α
(kDa) – 1 24 1 24 1 24 – Time (h)
150
100
65
50
NCC
SMC
COS7
g
Apoe−/−
Apoe−/−Ncc−/−
(kDa) – + – + IL18
250
150
100
75
50
NCC
h
Events
192
0
15 min
30 min
10^0 10^1 10^2 10^3
FL2H
pcDNA3.1 + biotin-IL18
NCC/pcDNA3.1 + biotin-IL18
NCC/PcDNA3.1 + heated biotin-IL18
Bound/free
3,200
3,000
2,800
2,600
2,400
2,200
0 5,000 10,000 15,000 20,000, 25,000
Bound (RFU)
Specific binding (RFU)
25,000
20,000
15,000
10,000
5,000
0
0 5 10
IL18 (nM)
Bmax = 62,260
Kd = 17.3
(kDa)
Vector + IL18
NCC + IL18
NCC + heated IL18
209
124
80
50
35
p-Tyr
β-Actin

Type of file: figure
Label: 3
Filename: figure_3.tif

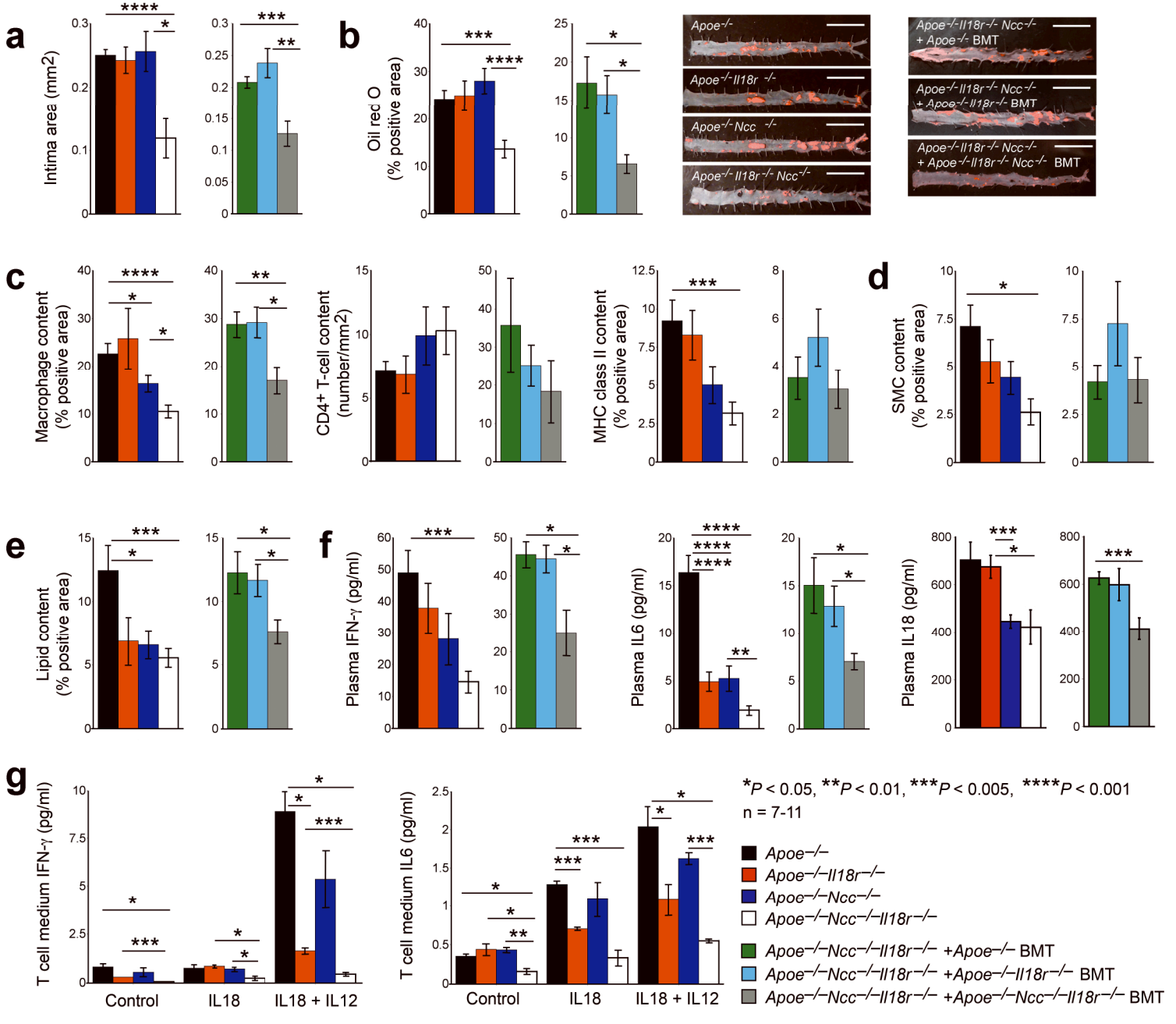
a
Intima area (mm2)
b
Oil red O (% positive area)
Apoe−/−
Apoe−/−Il18r −/−
Apoe−/−Ncc −/−
Apoe−/−Il18r−/− Ncc−/−
Apoe−/−Il18r−/− Ncc−/− + Apoe−/− BMT
Apoe−/−Il18r−/− Ncc−/− + Apoe−/−Il18r−/− BMT
Apoe−/−Il18r−/− Ncc−/− + Apoe−/−Il18r−/− Ncc−/− BMT
c
Macrophage content (% positive area)
CD4+ T-cell content (number/mm2)
MHC class II content (% positive area)
d
SMC content (% positive area)
e
Lipid content (% positive area)
f
Plasma IFN-γ (pg/ml)
Plasma IL6 (pg/ml)
Plasma IL18 (pg/ml)
g
T cell medium IFN-γ (pg/ml)
T cell medium IL6 (pg/ml)
Control
IL18
IL18 + IL12
*P < 0.05, **P < 0.01, ***P < 0.005, ****P < 0.001
n = 7-11
Apoe−/−
Apoe−/−Il18r−/−
Apoe−/−Ncc−/−
Apoe−/−Ncc−/−Il18r−/−
Apoe−/−Ncc−/−Il18r−/− +Apoe−/− BMT
Apoe−/−Ncc−/−Il18r−/− +Apoe−/−Il18r−/− BMT
Apoe−/−Ncc−/−Il18r−/− +Apoe−/−Ncc−/−Il18r−/− BMT

Type of file: figure
Label: 4
Filename: figure_4.tif

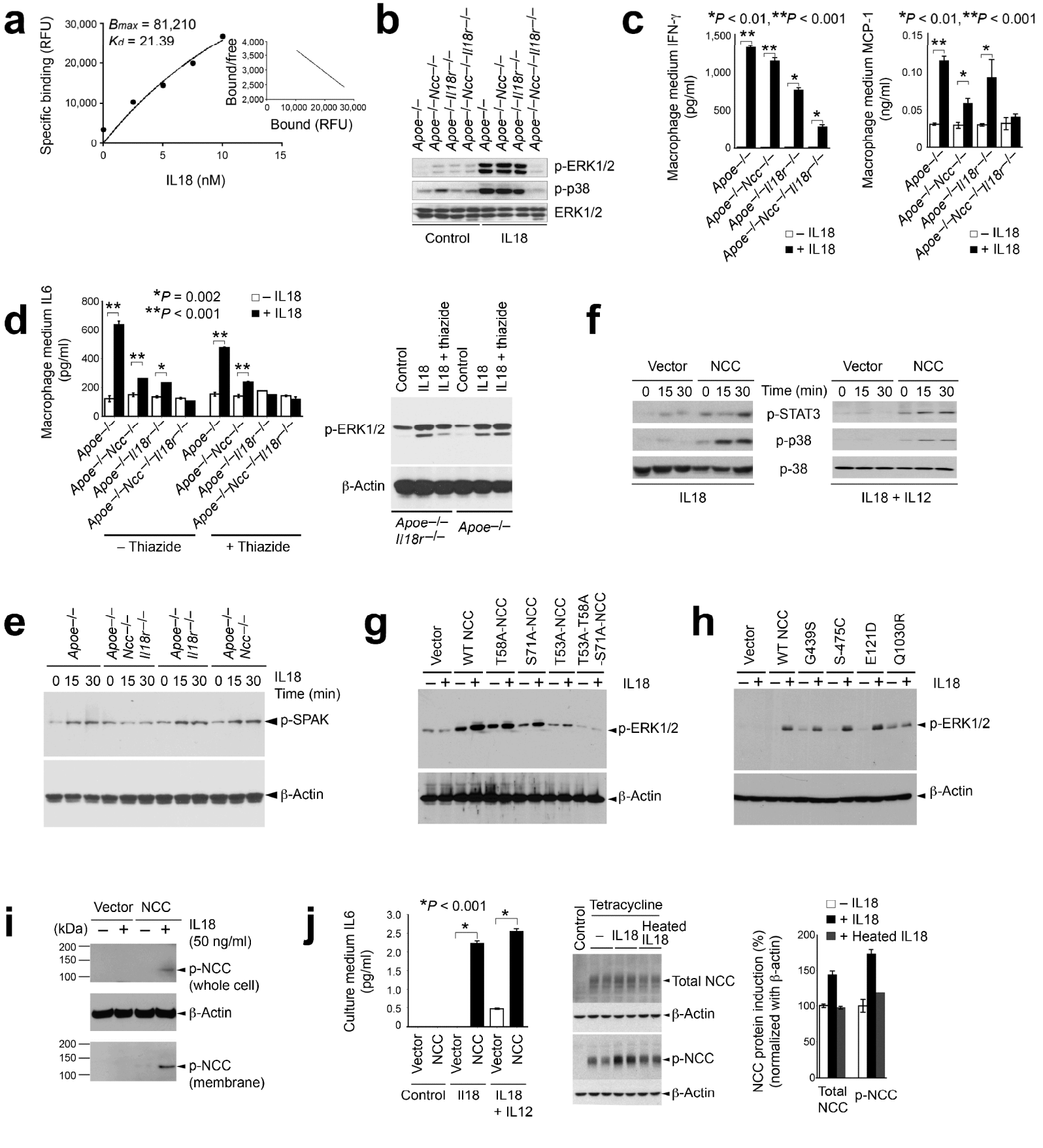
a
Specific binding (RFU)
Bmax = 81,210
Kd = 21.39
Bound/free
Bound (RFU)
IL18 (nM)
b
Apoe−/−
Apoe−/−Ncc−/−
Apoe−/−Il18r−/−
Apoe−/−Ncc−/−Il18r−/−
p-ERK1/2
p-p38
ERK1/2
Control
IL18
c
*P < 0.01, **P < 0.001
Macrophage medium IFN-γ (pg/ml)
Macrophage medium MCP-1 (ng/ml)
– IL18
+ IL18
d
*P = 0.002
**P < 0.001
Macrophage medium IL6 (pg/ml)
– Thiazide
+ Thiazide
Control
IL18
IL18 + thiazide
p-ERK1/2
β-Actin
Apoe−/−Il18r−/−
Apoe−/−
f
Vector
NCC
Time (min)
p-STAT3
p-p38
p-38
IL18
IL18 + IL12
e
p-SPAK
β-Actin
g
WT NCC
T58A-NCC
S71A-NCC
T53A-NCC
T53A-T58A-S71A-NCC
p-ERK1/2
β-Actin
h
WT NCC
G439S
S-475C
E121D
Q1030R
p-ERK1/2
β-Actin
i
(kDa)
IL18 (50 ng/ml)
p-NCC (whole cell)
β-Actin
p-NCC (membrane)
j
*P < 0.001
Culture medium IL6 (pg/ml)
Control
Il18
IL18 + IL12
Tetracycline
Heated IL18
Total NCC
p-NCC
NCC protein induction (%) (normalized with β-actin)
Total NCC
p-NCC